Table 5. Radiometer surface footprint resolution versus spacecraft altitude.

Spacecraft height (km)	Resolution	
	Along track (km)	Across track (km)
290	16	24
500	25	33
1000	44	50
2100	83	87

material and near-surface atmosphere. Thus, the temperature cannot change rapidly and is in adiabatic equilibrium; for a given elevation, the temperature is virtually the same everywhere: dark side to light side, pole to equator. Vertically, however, the temperature decreases at the adiabatic lapse rate of approximately -8 K km^{-1}. Thus, if we know the altitude of a surface region, we can immediately calculate its physical temperature, assuming it is in equilibrium with the overlying atmosphere (*14*). Because the Magellan altimetry experiment measures the height of the Venus surface, and does this with a lateral surface footprint resolution at least as small as that afforded to the emissivity determination by the 2° angular resolution of the HGA (Table 5), it is straightforward to calculate the actual physical temperature of the surface everywhere. The estimates of emissivity are included as entries in the ARCDR product, and are also resampled into a global emissivity image (GEDR), with 5-km pixels (Table 3).

A particularly interesting example of surface emissivity is from Maxwell Mons (Fig. 7). The area surrounding the Maxwell prominence is seen to be characterized by values of emissivity averaging about 0.85 (corresponding to a dielectric permittivity of 5), which are typical for the planet as a whole. At altitudes lying between 6055 and 6060 km radius, however, the emissivity drops rapidly to a low of 0.35, which requires a surface dielectric permittivity of 87. This general behavior has been noted before (*6*), but the resolution offered here allows a far more detailed look at the distribution of, and lower limits to, the values of emissivity in the Maxwell area. Interestingly, the northwest-southeast trending ridge to the left of the image center, where the altitude rises above 6060 to a maximum of 6062 km as noted earlier, shows emissivity increasing back to about 0.7. The reason for this apparent altitude dependence is not clear.

REFERENCES AND NOTES

1. The effective slant range, as also the along-track Doppler, resolutions given in Table 1 are determined as the half-power width of the response of the system to an echo from a point target (the point-spread, or ambiguity, function) and are approximately 0.4 times the inverse of the half-power width of the corresponding modulation transfer function. In the Magellan radar, the slant range resolution has been broadened, as compared to the theoretical value for the modulation bandwidth used, in order to reduce the variation in response against delay that would otherwise have been seen when sampling a point target echo at intervals of the reciprocal modulation bandwidth.
2. A detailed description of the radar system's operation is given by W. T. K. Johnson, *Proc. IEEE*, in press.
3. All of the MIDR products will become available to the general planetary and geological community through NASA's Space Science Data Center and its Planetary Data System, after they have been validated by the Magellan Project and scientific team.
4. T. Hagfors, *Radio Sci.* **5**, 189 (1970).
5. Figure 2 in J. W. Head *et al.*, *Science*, **252**, 276 (1991).
6. G. H. Pettengill, P. G. Ford, B. D. Chapman, *J. Geophys. Res.* **93**, 14,885 (1988).
7. Figure 16 in J. W. Head *et al.*, *Science* **252**, 276 (1991).
8. The pulse repetition rate (PRF) is fixed at 14,957 s^{-1} in the altimetric mode. Range aliasing (at delay multiples of 67 μs) within the antenna's illumination pattern becomes serious primarily at high altitudes, but even there it is important only for high values of positive or negative Doppler shifts along track, near the limits of the altimeter antenna response at an incidence angle of 5°. Doppler aliasing (at multiples of the PRF) is only important at low altitudes, where the spacecraft's orbital velocity is high. Rejection of data corresponding to highly Doppler-shifted surface footprints, which have incidence angles of more than a few degrees, relieves both problems.
9. In this approach, the mean received noise power, and its fluctuation in the absence of echo, are first estimated and used to establish a threshold. The position of the earliest significant echo power to exceed this threshold is then noted and reported as the surface height. No attempt has been made to refine the along-track dimension of the surface footprint through Doppler resolution.
10. See G. L. Tyler *et al.*, *Science* **252** 265 (1991).
11. At lower altitudes, the data are combined to broaden the effective along-track resolution to about 8 km in order to reduce statistical fluctuation ("speckle").
12. Note that beam efficiency is not the same thing as aperture effjciency, which is related to the point-source gain of the antenna and is known reasonably well, but which is not particularly helpful in interpreting filled-beam radiometry measurements.
13. Based on the Venus International Reference Atmosphere, issued by COSPAR, as vol. 5, No.11, of *Adv. Space Res.* (1985).
14. The mean thermal gradient down into the subsurface material is approximately 25 K km^{-1}, and the penetration of rdio waves through this near-surface material is likely not to exceed a few tens of meters; thus, with acceptable error, we can reasonably assume that the physical temperature for the emitting region is the same as for the surface and immediately overlying atmosphere.
15. D. O. Muhleman, *Astron. J.* **69**, 34, (1964).

16. We thank the entire Magellan Project staff for bringing the experimental techniques and measurements described here to successful fruition over many years of effort. Particular individuals who deserve mention are P. Graf, S. Lewicki, F. Liu, and J. Quigley.

10 January 1991; accepted 20 February 1991

Magellan: Electrical and Physical Properties of Venus' Surface

G. LEONARD TYLER, PETER G. FORD, DONALD B. CAMPBELL, CHARLES ELACHI, GORDON H. PETTENGILL, RICHARD A. SIMPSON

Magellan probes Venus' surface by 12.6-cm-wavelength vertical and oblique radar scattering and measures microwave thermal emission. Emissivity and root-mean-square slope maps between 330° and 30°E and 90°N and 80°S are dissimilar, although some local features are exceptions. Inferred surface emissivities typically are ~0.85, but vary from ~0.35 at Maxwell to ~0.95 northeast of Gula Mons and other locations. Lowest emissivities appear in topographically high areas; this relation suggests that a phase change or differences in chemical weathering occur at about 6055-kilometer radius. Initial results indicate that there are significant variations in the surface scattering function.

WITH THE EXCEPTION OF A SMALL number of locations examined by landing spacecraft (*1*), knowledge of the physical properties of Venus' surface must be inferred from observations of electromagnetic radiation either scattered or emitted by the surface. In the case of Magellan, interpretation is primarily from radar images and by classical geologic mapping techniques adapted for radar geometrical effects and large-scale scattering. Interpretation also involves determination of electromagnetic properties of the surface material and estimates of its physical structure from nonimaging data; these measurements serve as constraints and tests on geological hypotheses (*2–9*). In this report we describe, for the first 38 days (301 orbits) of Magellan operations, 12.6-cm-wavelength (λ) scattering and thermal-emission data and discuss possible inferences for Venus' surface properties. Our inferences apply to the statistical properties of the surface on wavelength-related scales but averaged over areas that at present are minimally of the order 100 km^2 (*10*).

Earlier observations were carried out at λ = 17 cm by the Pioneer Venus Orbiter,

G. L. Tyler and R. A. Simpson, Stanford University, Stanford, CA 94305.
P. G. Ford and G. H. Pettengill, Massachusetts Institute of Technology, Cambridge, MA 02139.
D. B. Campbell, Cornell University, Ithaca, NY 14853.
C. Elachi, Jet Propulsion Laboratory, Pasadena, CA 91109.

albeit at much coarser resolution and with less accuracy (*11–13*). Venera 15 and 16 obtained altimetry and radar images at $\lambda = 8$ cm of Venus north of about 30°N and radiometric data north of the equator (*14, 15*). These spacecraft observations built on and complemented a long series of ground-based measurements and maps produced at $\lambda \approx 12.6$ cm (*5, 6, 16, 17*). The earlier observations showed that the intrinsic reflectivity of Venus' surface is on average equivalent to the Fresnel power reflection coefficient at normal incidence of about $\rho_0 = 0.13$. Values range from a minimum of ~0.03 to >0.40; the highest values were observed only for areas at high elevations (*18*). The corresponding values of surface emissivity range from ~0.39 to 0.95 (*12*).

The overall reflectivity and emissivity of the surface can, with suitable modeling, be related to the electromagnetic properties of the material—its permittivity, permeability, and conductivity—whereas the variations in backscatter reflectivity and emissivity with viewing angle can be associated with the texture, or wavelength-scale morphology, of the surface. For incidence angles less than 40°, the surface backscattering properties are often modeled by the Hagfors scattering function (*19*)

$$\sigma_0(\theta_i) = \frac{\rho_0 C}{2}(\cos^4\theta_i + C\sin^2\theta_i)^{-3/2}$$

where $\sigma_0(\theta_i)$ is the specific backscatter cross section at incidence angle θ_i, ρ_0 is the Fresnel reflection coefficient of the surface, and C is a parameter related to the root-mean-square (rms) surface slopes for scales somewhat larger than λ. The rms slope is given approximately by $C^{-1/2}$. A value of $C \approx 175$, corresponding to an rms slope of ~4°, is typical (*5, 20*). Surface emissivity is taken as the complement of the Fresnel reflectivity with certain simplifying assumptions. The validity of this equation as well as the role of subsurface and multiple scattering (not included in the Hagfors formulation) are subjects of continuing study, but will not be discussed further here.

The Magellan radar system, although a single assembly, has three distinct modes for sensing Venus' surface. The Synthetic Aperture Radar (SAR) and Altimeter are active sensors that allow measurement of the surface backscatter reflectivity in oblique and near-nadir (vertical incidence angle) viewing geometries, respectively. The thermal emission of Venus at microwave frequencies is measured by sampling the SAR receiver output when there are no radar echoes present.

Magellan's SAR operates through the narrow beamwidth, high-gain antenna at angles of incidence between about 15° and 50° from the local surface normal. Incidence angles are smallest toward the poles and largest at periapsis, near 10°N latitude. The narrow SAR beamwidth limits observations to angles within about 1° of the beam center (Fig. 1).

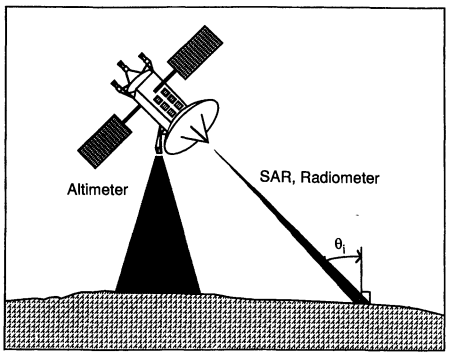

Fig. 1. Magellan geometry for imaging, radiometry, and altimetry. The SAR and radiometer view surface through 2.1° beamwidth antenna. Beam intercepts surface obliquely at incidence and emission angle θ_i; spacecraft rocks slowly (in plane of figure) with position in orbit causing θ_i to vary from about 15° near Venus' north pole, to about 50° at 10°N, which corresponds to orbital periapsis, to about 15° again near 80°S. Altimeter horn antenna, fixed at 25° angle with respect to SAR antenna, is directed generally toward nadir; broad beam, approximately 30° in plane of figure, allows collection of scattered signal from a range of incidence angles (see Fig. 2).

Radiometer measurements provide an estimate of the thermal microwave power emitted by the surface of Venus in the direction of Magellan. This power is limited to that contained in the narrow range of angles associated with the SAR antenna beam (Fig. 1) (*21*) and to the narrow range of frequencies accepted by the radar receiver (*22*). The spacecraft receiver path has been calibrated to provide absolute power measurements so that interpretation in terms of surface physical constants is practical. One can derive the surface emissivity in the direction of the spacecraft from the measurement of received power by modeling the contribution from the atmosphere and from the sky and by assuming that the surface temperature is the same as that of the adjacent atmosphere (*4*).

Altimetry is achieved by a brief diversion of the radar energy to a broad beamwidth, horn antenna that is aimed roughly toward the nadir (Fig. 1). Approximately once each second, a burst of 17 radar pulses is transmitted downward and the corresponding echoes are received. The system operated in this manner has been optimized primarily for determination of range to the surface. In principle the altimeter provides continuous angular coverage from the nadir—corresponding to an angle of incidence of 0°—to the limits of the altimeter antenna beam. The wide antenna beamwidth permits echoes from more than one pulse to be received simultaneously; however, unambiguous echoes are obtained only to an angle of incidence of about 6° near the poles and of about 15° at periapsis (*23*).

Figure 2 gives the scattering angles observed with the altimeter and the SAR as compared with the Hagfors scattering law and Fresnel emissivity (compare with Fig. 1). Whereas the altimeter typically samples the region about the nadir, the angle of incidence of the SAR boresight can be located anywhere within a wide range corresponding to the viewing geometry chosen. For any choice of SAR incidence angle the observed emission angle is the same.

The methods of data reduction utilized to obtain the scattering cross section for the

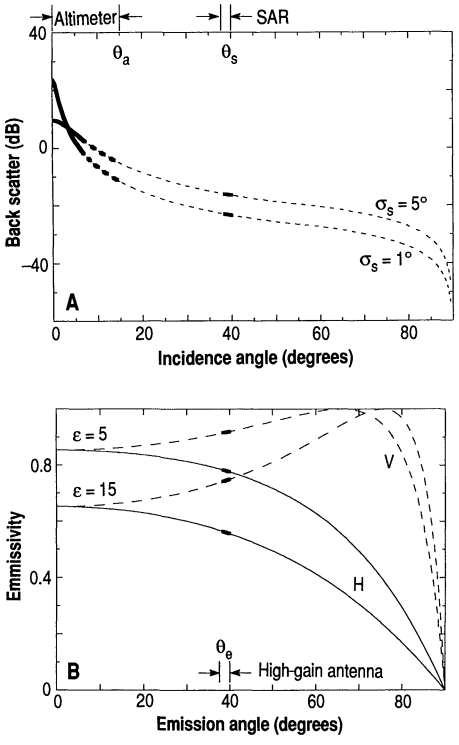

Fig. 2. Examples of scattering cross-section (**A**) and emission (**B**) curves illustrating parts sampled by Magellan. Altimeter obtains unambiguous scattering data to about $\theta_a = 6°$ near the poles and to about $\theta_a = 15°$ near the equator. SAR obtains scattered signal from within 1° to 2° of incidence-angle ranges somewhere within $15° < \theta_i = \theta_s < 50°$. Thermal emission is received from a small range of angles around $\theta_i = \theta_e$. Strength of the emission signal depends on the constitutive properties of surface material, here illustrated for two different values of dielectric constant (ε), the polarization of the receiving antenna (H or V), and the physical surface temperature. Magellan currently is using horizontal (H) polarization (electric-field vector parallel to surface); vertical (V) polarization requires 90° rotation of the spacecraft about the high-gain antenna boresight. Surface roughness modifies the idealized emission curves somewhat.

SAR geometry are straightforward. For known transmitter power, receiver sensitivity, and viewing conditions, measured receiver power can be reduced to estimates of specific backscatter cross section $\sigma_0(\theta_i)$ (*4, 7, 24*). Similarly, although there are calibration issues specific to the Magellan instrument, the reduction of the radiometer data followed standard practices (*4, 25*). In both cases atmospheric attenuation and refraction were corrected, and a standard topographic model derived from Pioneer Venus data was used to account for large-scale elevation changes.

Two independent approaches for reduction of the altimetry data have been used for Magellan. The first is directed toward extraction of topographic information as well as surface properties (*4*). Under the assumption of the Hagfors scattering law, the shape and strength of the echoes are modeled as a function of the surface rms slope and intrinsic reflectivity; these two parameters are extracted simultaneously by selection of the member of a precomputed family of curves that best fits the observation. The time at which the best fit occurs provides the radar range. Subtraction of the spacecraft-to-surface range from the spacecraft-to-Venus center-of-mass distance yields the surface radius immediately under the radar and, hence, the topography. Essentially, the surface roughness is determined from the time dispersion of the echo, and the echo strength provides an estimate of the reflectivity. The reflection coefficient of the surface material can be obtained by adjustment of the estimated received power for the fraction of a surface resolution cell that scatters diffusely because of the small-scale surface structure. This plus other necessary corrections have not been carried out yet. Surface resolution is determined by a combination of the scattering properties and the radar characteristics. Similar approaches have been employed in Earth-based radar observations of Mars (*26*) and in the reduction of Pioneer Venus data (*12*). Strengths of this approach include rapid, uniform determination of the surface topography and a measure of the surface physical and electromagnetic properties.

An alternative approach yields surface information without need for selection of a particular scattering model. This technique relies on use of intrinsic geometrical constraints that can be enforced on the altimeter data by signal processing. For example, reception of an altimeter echo signal at a specific Doppler frequency implies that it arose from a locus of points on the surface of Venus defined by the spacecraft position and a fixed angle with respect to the spacecraft velocity vector (*27*). Modeling of the geometric aspects of the altimeter observations such as those giving rise to the echo spectrum, time delay, or delay-Doppler spectrum is sufficient to permit a solution for the surface scattering law without a priori assumption as to its form (*28*). This method has been applied to limited observations of the moon and Mars (*29–31*). Use of the technique can decrease sensitivity to height variations within the altimeter footprint, allows detection of changes in surface morphology expressed as differing functional forms for surface statistics, and reduces the number of assumptions. For Magellan, discrete forms of the integral equations relating the surface scattering function and the observed time delay and power spectrum of the echo signals have been used. The linearized equations were solved to find the scattering function that simultaneously provides the best rms fit to echo time delay and power spectrum corresponding to a given scattering region. Combining these two data types yields a more robust solution than can be had with either type alone.

The observations encompass major structures such as Ishtar Terra, Maxwell Montes, and Eistla Regio, but in total area is dominated by the lowland plains of Sedna, Guin-

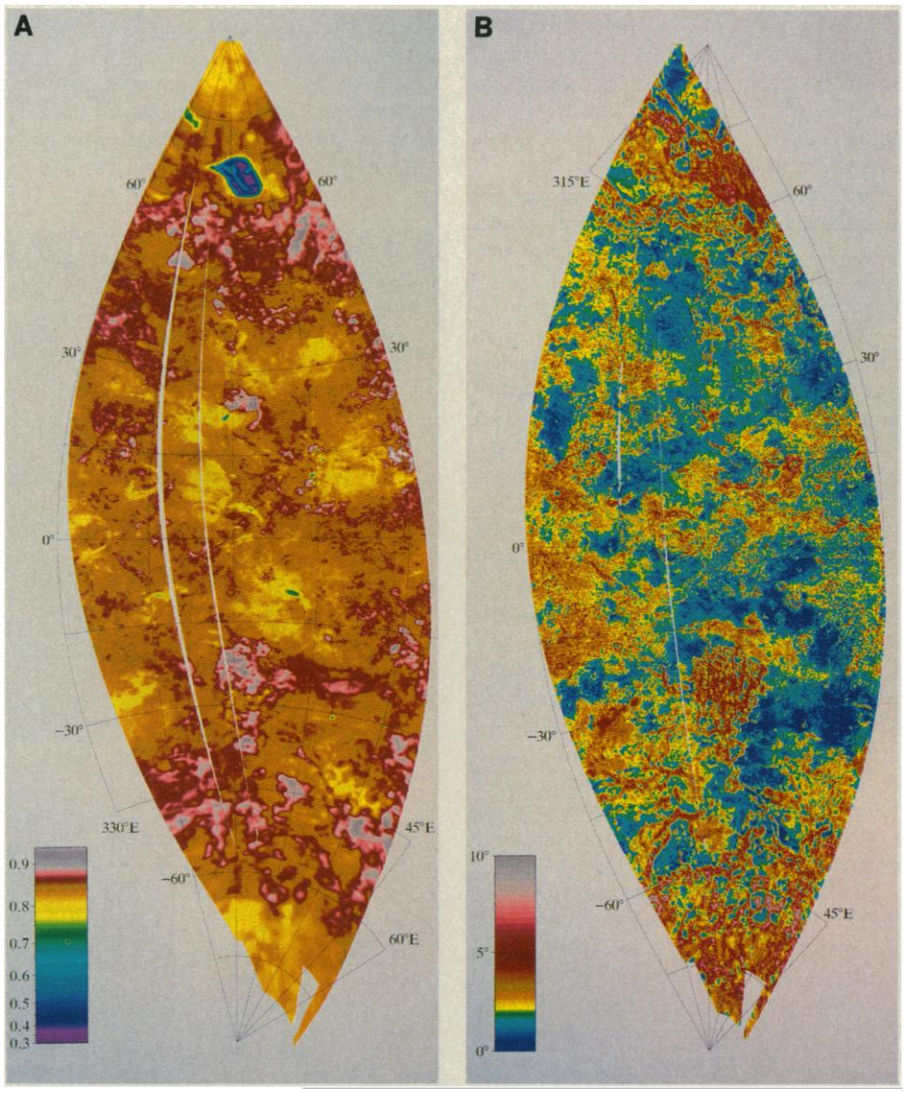

Fig. 3. Venus (**A**) surface emission and (**B**) rms slopes inferred from Magellan observations. Sectors shown lie between about 330° and 30°E longitude and 90°N and 80°S latitude in a transverse Mercator projection, centered on the prime meridian. Emissivity is based on measurement of thermally radiated microwave energy at $\lambda = 12.6$ cm and assumptions that the surface is planar and in thermal equilibrium with the atmosphere after correction for topographic altitude variations. Root-mean square slopes are based on time dispersion of altimeter echoes. For surface emissivity (A), lateral resolution varies from approximately 14 km (north to south) by 20 km (east to west) near periapsis (10°N) to approximately 75 by 75 km near the north pole and 80°S. For rms slope (B) the resolution is of the order of 10 km at periapsis and increases by approximately a factor of 2 near the extremes, as above. These resolutions are substantially more coarse than those achieved by the SAR, but are considerably finer overall than resolutions achieved by earlier spacecraft or from Earth (*11, 33*).

evere, and Lavinia Planitiae. Quantitative analysis is limited to study of the altimeter echo time and frequency dispersion and of the radiometry data. Interpretation is in the context of radar backscatter variations that form the SAR images; for the reasons indicated above, the use of absolute backscatter signal strengths has not been incorporated (*32*).

Typical values for the emissivity are ~0.85. These are consistent with rock or with highly consolidated soil comprising closely packed fine rock fragments; they are inconsistent with more porous surfaces such as the lunar regolith or Martian sands. Typical values of rms slope are 2.5° ± 0.5° in plains areas and somewhat larger elsewhere; the maximum value of roughness that can be sensed reliably at present is about 6.5°, which occurs in many tessera terrains. As can be seen from Fig. 3, however, both emissivity and rms slope vary considerably over the surface.

Patterns evident in the emission and rms slope measurements are markedly dissimilar (Fig. 3). This dissimilarity suggests that these parameters represent independent attributes of the surface. In general, the dissimilarity is evident on all scales depicted, to the limits of resolution. Values of either data type are correlated locally over scales of hundreds of kilometers (compare Figs. 3, A and B). This correlation gives rise to the somewhat patchy appearance of each pattern and suggests that some regional surface units have common properties and common origins.

Maxwell Montes, centered at about 65°N, 5°E, has an inferred emissivity that is strikingly low and distinct from that of its environs (*4*) (the prominent teardrop-shaped feature near the top of Fig. 3A). The summit of Maxwell Montes is the highest known point on Venus (*34*). Maxwell is also rougher than the Venus norm (Fig. 3B), but its roughness does not differ from that of the neighboring Fortuna Tessera to the same extent as its emissivity.

Sedna Planitia, which extends from about 50°N, 315°E southeast to about 30°N, 0°E, is a major lowland plains area with typical values of rms slope of 2.6 ± 0.5° and emissivity of 0.83 to 0.87. Sedna Planitia is defined poorly in the emissivity and rms slope data (Fig. 3), although it is a prominent topographic feature (*4*) and is evident in the SAR images.

"Horned" features, parabolic-shaped structures opening to the west, appear in several places (for example, at approximately 10°N, 342°E, extending 6° north to south and east to west) in the emissivity data (Fig. 3A), and a few can be seen in the SAR images (*35*); they are not readily discernible in the rms slope data, although subsections of the horns can be found in some cases (Fig. 3B).

Some features can be identified readily in both emission and rms slope. For example, a feature southwest of Maxwell, centered at 49.5°N, 346°E and extending about 3.5° north to south by 7° east to west, resembles Australia in shape. It appears as a compact region of relatively high emissivity (~0.91). Values of rms slope are typically 4° and locally reach 6°. This particular area is too small to appear prominently in the earlier Pioneer Venus emissivity and rms slope measurements, nor is it distinguished in the Venera 15–16 maps (incidence angle 10°); but it is readily apparent in early Arecibo images at an incidence angle of approximately 50° (*5*).

One of the most prominent features known from Earth-based maps, Alpha Regio, has both moderately high emissivity and a high rms slope, although it is not so clearly delineated as the Australia-shaped feature to the north. Centered at approximately 25°S and 5°E, it has emissivity of 0.88 to 0.92, and rms slopes in the range of 4.5° to 6.5°.

The area near Sif Mons and Gula Mons, centered at approximately 22°N, 355°E, indicates that there are several systematic relations in detail among emissivity, rms slope, topography, and surface deposits on Venus. These are volcanic edifices situated in Eistla Regio, an upland region extending to the west some 7000 km from Aphrodite Terra and rising to about 1.5 km above mean planetary radius. Sif Mons rises 2 km above Eistla Regio and possesses a classical shield-volcanic form centered on a 50-km-diameter circular structure at its summit. Emanating from this central area, and from other sources nearby, are many volcanic flow deposits extending up to 500 km from the summit (*36*). Gula Mons, 700 km to the east of Sif

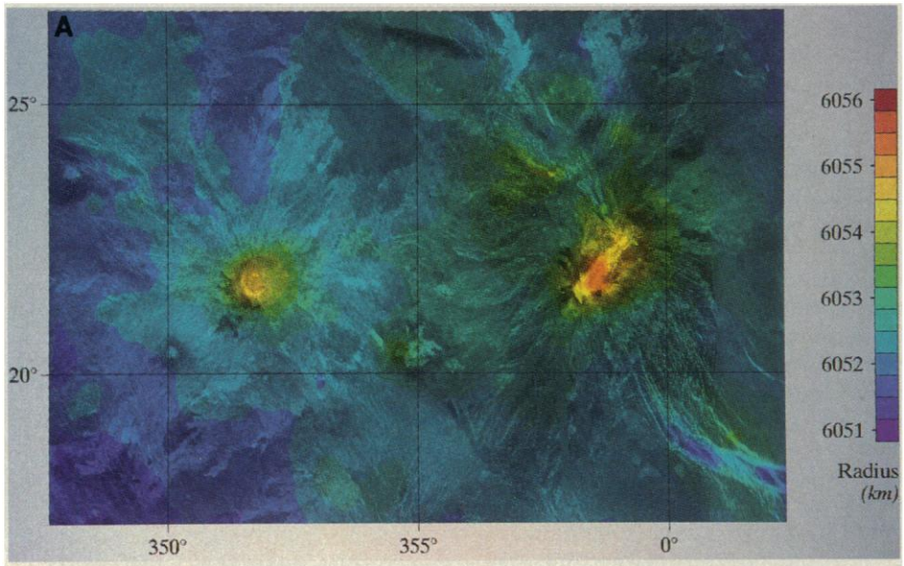

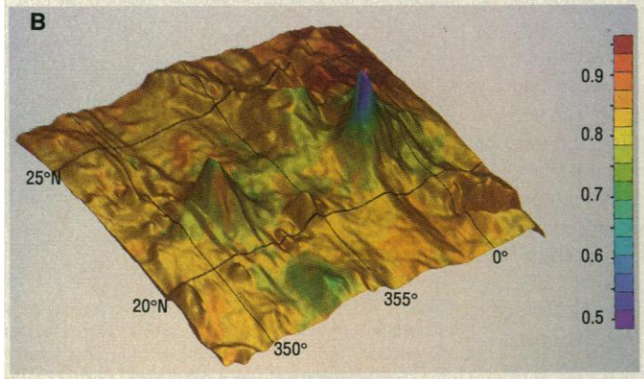

Fig. 4. Sif and Gula Montes: radar brightness, topography, and emission. (**A**) Magellan SAR backscatter of Sif and Gula area, mapped as brightness with topography superposed as color. In a few places (for example, for longitudes east of 1°E) Arecibo image data have been inserted where Magellan SAR images were not available. (**B**) Shaded relief map depicting topography with emissivity superposed as color. Sector shown is centered at approximately 22°N, 355°E and extends ~1500 km east to west by ~1000 km north to south. Entire region of figure lies in Eistla Regio, which is about 1.5 km above mean planetary radius. In (A), note radar brightness of flows emanating from central circular structures, and extreme radar brightness of summits of Sif and Gula. In (B), note relatively low value of emissivity inferred for summits, corresponding to location of high SAR backscatter in (A), and high emissivity at approximately 25°N, 0°E, for which there is no apparent corresponding structure in the SAR backscatter result (see text).

Mons, rises 3 km above Eistla Regio. The SAR image of Gula Mons (Fig. 4A) indicates that radial deposits on Gula are less well developed than on Sif Mons. Two radar-bright, flow-like surfaces can be seen to the north and northwest of Gula; these extend for several hundred kilometers. A third bright deposit about 100 km in extent lies on the summit region of the mountain.

The high SAR brightness of the Sif and Gula deposits could be due to an increase in the level of diffuse scatter associated with greater surface roughness, but it also could be associated with differences in the composition of these deposits relative to the surrounding terrain (*37*). The bright deposit at the summit of Gula Mons has a low thermal emission (~0.55). This low emission, which we interpret as indicating the presence of a surface layer with an average dielectric constant of 25 or greater—a high value compared with the Venus average of about 5 (*38*)—occurs at the same location as the high radar return in the SAR image (Fig. 4A). An examination of the topography of Gula Mons indicates that the area of low emission outlines the approximately 6054.0-km-radius contour, which is 2.1 km above mean planetary radius and extends to the summit located at a radius of 6056 km. Another area of significantly low emissivity corresponds to the circular summit structure of Sif Mons, where the emissivity is ~0.70 as compared with the average value of about 0.80 for the surrounding area. Perhaps significantly, this area also lies mostly above the 6054.0-km-radius contour; the summit of Sif is at 6054.5 km. A similar relation is observed at Maxwell (*4*), where the areas of reduced emissivity also occur above the 6055-km contour. This phenomenon may be globally related to a phase transition or chemical weathering process that depends on atmospheric temperature or pressure (*39*). There are also a few small areas of reduced emissivity at lower elevations, however.

The highest value of inferred emissivity in the Sif Mons–Gula Mons area is ~0.95 over a small area to the northeast of the summit of Gula Mons (Fig. 4B). There is no bright feature at this location in the SAR image; thus, this high value likely is not caused by locally increased surface roughness. This lack of correspondence is observed for several prominent features in the emissivity image northeast of Gula and may indicate changes in surface composition that are related only weakly to the structures observed in SAR images.

There is clear correspondence between the emissivity data and the SAR image in the radial flow-like deposits of Sif Mons. The outer extents of many of the flows have enhanced emissivities, relative to the surroundings; values range up to 0.85 and, locally, to 0.89. This 5 to 10% increase in the emissivity may be associated with factors such as (i) variation in the surface texture of the flows caused by changing conditions as the flows cooled after ponding in the relatively flat terrain surrounding Sif Mons; (ii) changes in roughness resulting from erosion; or (iii) differences in the intrinsic composition of the flow material relative to the surrounding plains.

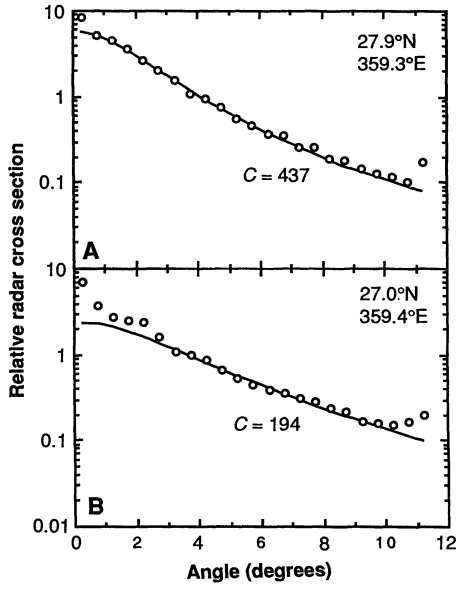

Fig. 5. Scattering functions for Venus north of Gula Mons. (**A**) 27.9°N, 359.3°E and (**B**) 27.0°N, 359.4°E. Solid curves represent Hagfors scattering function chosen for best fit to data over incidence angles 3° to 9° for each location. Results in (A) correspond closely to Hagfors law, while results in (B) deviate significantly for angles less than about 3°. Vertical scale is arbitrary, pending calibrations (see text).

Only a few orbits have been examined for variations in surface morphology as expressed in the radar scattering law. Radar scattering functions derived from altimetry data in two areas north of Gula Mons, located at 27.9°N, 359.3°E and 27.0°N, 359.4°E (Fig. 5), show that there is significant deviation from the Hagfors model at small incidence angles in some areas. The average rms slope for the area at 27.0°N is 4.1° (Fig. 5B), which is near Venus' average and typical of values obtained from the same orbit as the spacecraft passed near the summit of Gula Mons. Even though the rms value is typical, the form of the scattering function deviates significantly from the model at incidence angles <3°. In contrast, the rms slope corresponding to the Hagfors law at 27.9°N is about 2.7° (Fig. 5A), significantly less than Venus' average of 4°. A deviation from the Hagfors form at low angles is not evident in this area, however.

Hagfors (*19*) assumed that a surface could be characterized by Gaussian height statistics and an approximately exponential autocorrelation function. Evidently, the surface at 27.9°N contains a significantly larger proportion of nearly level facets than assumed in Hagfors' model; a similar conclusion has been drawn from some Mars radar data (*31*), whereas most areas of the moon fit the Hagfors model much better (*30*). By identifying anomalous regions, the Magellan data can be used to sense a wide variety of surface morphologies.

REFERENCES AND NOTES

1. C. P. Florensky *et al., Bull. Geol. Soc. Am.*, **88**, 1537 (1977); M. Ya. Marov, *Annu. Rev. Astron. Astrophys.* **16**, 141 (1978); C. P. Florensky *et al., Science* **221**, 57 (1983); Yu. A. Surkov *et al., J. Geophys. Res.* **89**, B393 (1984); Yu. A. Surkov *et al., ibid.* **91**, E215 (1986).
2. Radar images depict variations in backscatter strength on fine lateral scales; for Magellan the linear resolution of the SAR is of the order of 100 m. The scattering and emissive properties of the surface are controlled by structure on wavelength-related scales well below the resolution element in size and by the constitutive parameters of the surface material. Inferences regarding these small scales and material properties can be derived from quantitative study of the scattering and emission. The Magellan approach is described in (*3*) and (*4*). Earlier studies of Venus based on the use of radar data and that illustrate the complementary nature of the classical geologic and quantitative approaches are in (*5*) and (*6*). Wave interactions with materials are discussed widely in texts on electromagnetic theory. For a development in a remote sensing context see (*7*). For application to planetary problems see J. V. Evans and T. Hagfors, *Radar Astronomy* (McGraw-Hill, New York, 1968).
3. R. S. Saunders *et al., J. Geophys. Res.* **95**, 8339 (1990).
4. G. H. Pettengill *et al., Science* **252**, 260 (1991).
5. D. B. Campbell and B. A. Burns, *J. Geophys. Res.* **85**, 8271 (1980).
6. D. B. Campbell *et al., Science* **246**, 373 (1989); H. Masursky *et al., J. Geophys. Res.* **85**, 8232 (1980).
7. F. T. Ulaby, R. K. Moore, A. K. Fung, *Microwave Remote Sensing* (Addison-Wesley, vol. 1 and 2, Reading, MA, 1981 and 1982).
8. The use of radar data for geologic study has been established previously. For example, it has been demonstrated for the moon that small-scale surface statistics sensed by radio wave scattering provide a measure of relative surface age (*9*).
9. H. J. Moore and G. L. Tyler, "Comparison Between Photogrammetric and Bistatic Radar Slope Frequency Distributions, Apollo 17 Preliminary Science Report" (*NASA SP-330*, U.S. Government Printing Office, Washington, DC, 1973), chap. 33-17; H. J. Moore *et al., U.S. Geol. Surv. Open-File Rep. 75-284* (1975); H. J. Moore *et al., ibid. 76-298* (1976); G. L. Tyler, *Icarus* **37**, 29 (1979).
10. Waves interact most strongly with structures having dimensions of a few tenths of a wavelength to many wavelengths, but the radiometer and altimeter measurements of interest here have spatial resolutions no better than a few kilometers. The measurements thus represent the composite response of many statistically independent radiating elements in each spatial resolution cell. An introduction and overview can be found in G. T. Ruck, D. E. Barrick, W. D. Stuart, C. K. Krichbaum, *Radar Cross Section Handbook* (Plenum, New York, 1970), chap. 9. The scattering model is based on a spherical surface, representing Venus, of uniform statistics and effectively no height variations.
11. Lateral resolution of Pioneer Venus altimetry varied from approximately 7 by 23 km near periapsis to about 100 by 100 km at polar latitudes.
12. G. H. Pettengill, P. G. Ford, B. D. Chapman, *J.*

Geophys. Res. **93**, 14881 (1988).
13. G. H. Pettengill, P. G. Ford, S. Nozette, *Science* **217**, 640 (1982); P. G. Ford and G. H. Pettengill, *ibid.*, p. 220.
14. V. L. Barsukov *et al.*, *J. Geophys. Res.* **91**, D378 (1986); A. T. Basilevsky *et al.*, *ibid.*, p. D399; B. A. Ivanov *et al.*, *ibid.*, p. D413.
15. Yu. N. Alexandrov *et al.*, *Science* **231**, 1271 (1986).
16. R. M. Goldstein *et al.*, *Icarus* **36**, 334 (1978); R. F. Jurgens, R. M. Goldstein, H. R. Rumsey, R. R. Green, *J. Geophys. Res.*, **85**, 8282 (1980); R. F. Jurgens *et al.*, *Geophys. Res. Lett.* **15**, 577 (1988).
17. P. G. Ford and D. A. Senske, *Geophys. Res. Lett.* **17**, 1361 (1990).
18. Six elevated regions observed by Pioneer Venus at a wavelength of 17 cm (Ovda Regio, Thetis Regio, Maat Mons, Ozza Mons, Theia Mons, and Rhea Mons) have an average surface reflection coefficient of 0.39 ± 0.03 and an average surface emissivity of 0.61 ± 0.11, where the indicated variation is 1 SD of the reported values in tables 2 and 3 of (*12*). Also see R. Arvidson, Ed., *Pre-Magellan Radar and Gravity Data* (*USA NASA JPL MG-1001*, Planetary Data System, NASA, Washington, DC, 1990).
19. The Hagfors law is from T. Hagfors, *J. Geophys. Res.* **69**, 3779 (1964). The close relation between the physical-geometric optics formulation and quasi-specular scatter, which forms the basis for much of the geological interpretation of planetary radar data, is given in T. Hagfors, *J. Geophys. Res.* **71**, 379 (1966). The approximate relation between rms surface slope and the Hagfors parameter C is derived in "Radar Studies of the Moon" (*Final Rep.*, vol. 1, Lincoln Laboratory, Lexington, MA, 1967). Generally for models of natural surfaces, inferred rms slopes refer to a smoothed version of the actual surface, that is, to the long-wavelength portion of the surface height spectrum. The "filtering" process by which the effective portion of the spectrum is selected is not well-understood. Also, see (*20*).
20. The horizontal scale to which an rms slope measurement applies depends on several factors, including the height spectrum of the surface [G. L. Tyler, *Radio Sci.* **11**, 83 (1976)]. Empirical comparison of radar results with photoclinometric and photogrammetric estimates of lunar slopes suggests that the radar rms slope is an effective value representing an average over scales from a few to a few hundred wavelengths (*9*), hence the range quoted for Magellan.
21. Use of the spacecraft high-gain antenna for radiometry effectively limits the range of emission angles sensed to the antenna beamwidth, which is slightly over 2°, one way, full width at the half-power response points. Observations represent beam-weighted averages about the mean angle. The angle of the beam axis with respect to the surface varies, depending on the programming of the SAR observations. For the primary mission, a minimum emission angle of about 17° obtains near the north pole, whereas the value near periapsis at 10°N is 47°. The situation is slightly different for the SAR as range processing of the radar echoes provides the ability to discriminate echoes as a function of angle independently of the antenna characteristics. In principle it is possible to measure the variation of the echo strength with scattering angle, and hence to estimate the slope of the scattering law across the SAR swath as well as the average value. Whether this can be achieved in a meaningful way in practice, given changes in the surface characteristics evident in many of the SAR images, remains to be seen. In any event the scattering law is expected to be well constrained by the measurements about the nadir plus at least one constraining value at moderate values of the angle of incidence (compare Figs. 1 and 2).
22. The bandwidth for radiometry is 10 MHz, detected and accumulated for 50 ms, yielding a time-bandwidth product of 5×10^5. The radiometry signal is obtained alternately from the high-gain antenna and from a comparison load at known temperature. In this way variations in receiver gain can be compensated relatively accurately over short time intervals to a precision of about 2 K; the absolute accuracy is about 15 K.
23. The half-power half-beamwidth of the altimetry antenna is about 5° in the direction of spacecraft motion and about 15° at right angles to the orbit plane. The useful range of incidence angles sensed depends on several factors, some of which change with position along the orbital track. At the highest altitudes, over the polar regions, altimeter echoes are aliased in the frequency domain at a folding point corresponding to about 7° angle of incidence, and in the time domain at a folding point corresponding to about 6° angle of incidence. Near periapsis, these values are about 3.3° and 15° angle of incidence, respectively. Superposition of echoes from different pulses, or range aliasing, is unavoidable, but in some circumstances the antenna pattern can be used to ensure that echoes from distant parts of the surface will be weak. In others, the scattering function itself guarantees that near-nadir echoes dominate.
24. Calibration of the SAR backscatter is based on the radar equation, laboratory measurements of the SAR system parameters, and tests for internal consistency of the data.
25. L. Tsang, J. A. Kong, R. T. Shin, *Theory of Microwave Remote Sensing*, (Wiley, New York, 1985). In obtaining the value of emissivity from the data, it is assumed that the surface is in thermal equilibrium with the atmosphere (*4*).
26. G. S. Downs, R. M. Goldstein, R. R. Green, G. A. Morris, P. E. Reichley, *Icarus* **18**, 8 (1973); G. H. Pettengill, I. I. Shapiro, A. E. E. Rogers, *ibid.*, p. 22.
27. G. L. Tyler and D. H. H. Ingalls, *J. Geophys. Res.* **76**, 4775 (1971).
28. M. N. Parker, thesis, Stanford University, Palo Alto, CA (1973); B. J. Lipa, and G. L. Tyler, *Icarus* **28**, 301 (1976).
29. M. N. Parker and G. L. Tyler, *Radio Sci.* **8**, 177 (1973).
30. R. A. Simpson and G. L. Tyler, *IEEE Trans.* **AP-30**, 438 (1982).
31. R. A. Simpson, G. L. Tyler, G. G. Schaber, *J. Geophys. Res.* **89**, 10385 (1984).
32. Full analysis requires calibration of both the SAR and altimeter data and estimation of scattering efficiency at angles not observed by either (Fig. 2).
33. Pioneer Venus resolution of radiometric observations varied from approximately 90 km at periapsis to more than 1000 km at the highest operating altitudes. The best emissivity measurements from Earth have resolutions of a few hundred kilometers.
34. The highest reported point lies at 64°N, 2°E, [G. H. Pettengill *et al.*, *J. Geophys. Res.* **85**, 8261 (1980)]. Also, see (*15*).
35. Horned features are postulated to result from wind-carried ejecta associated with impact processes [R. E. Arvidson *et al.*, *Science* **252**, 270 (1991)].
36. J. W. Head *et al.*, *Science* **252**, 276 (1991); D. B. Campbell *et al.*, *ibid.* **246**, 373 (1989).
37. Changes in surface composition that enhances horizontally polarized radar backscatter do so for all incidence angles, whereas enhancements at high incidence angles resulting from increased roughness will be offset by a decrease in radar backscatter near the nadir. Comparison of $\sigma_0(\theta_i)$ measurements from the SAR and altimeter, in conjunction with emissivity measurement, permits separation of roughness and composition effects.
38. Pettengill *et al.* (*12*) report a lowlands average radar reflectivity of 0.14, corresponding to an effective dielectric constant of 5.0; values for reflectivity in highlands regions vary from more than 0.4 (dielectric constant >20) for Maxwell Montes to typical values in the range of 0.35 to 0.40 (dielectric constant 15 to 20) for the six features named in (*18*). We quote values for dielectric constant calculated for a lossless material with relative permeability of unity for convenience only. There is no intent to imply that the actual material is so ideal.
39. At 6055 km the atmospheric temperature and pressure are 712.4 K and 76.01 bars, respectively; at the reference radius of 6051 km they are 743.0 K and 98.12 bars [A. J. Kliore, V. I. Moroz, G. M. Kesting, *Adv. Space Res.* **5**, 11 (1985)].
40. This work has been made possible by the dedicated efforts of many people associated with the Magellan Project at the Jet Propulsion Laboratory and at the authors' home institutions. We especially thank W. T. K. Johnson and P. Graf. We also thank F. Liu, J. Quigley, and M. Maurer.

8 January 1991; accepted 14 March 1991

Magellan: Initial Analysis of Venus Surface Modification

R. E. ARVIDSON, V. R. BAKER, C. ELACHI, R. S. SAUNDERS, J. A. WOOD

Initial Magellan observations reveal a planet with high dielectric constant materials exposed preferentially in elevated regions with high slopes, ejecta deposits extending up to 1000 kilometers to the west of several impact craters, windblown deposits and features in areas where there are both obstacles and a source of particulate material, and evidence for slow, steady degradation by atmosphere-surface interactions and mass movements.

RADAR OBSERVATIONS OF VENUS made by the Earth-based Arecibo and Goldstone facilities and by the Venera 15–16 spacecraft demonstrated that volcanic and tectonic landforms dominate the surface of that planet (*1*). However, the nature and extent of landform modification by such processes as chemical and mechanical weathering, eolian (that is, wind-related) processes, and mass wasting have remained unclear. The reason is that the spatial resolution of these observations is too coarse to resolve the relatively fine-scale features produced by such processes. For example, simulations with the use of Seasat radar images of Earth showed that the Gran Desierto dunes, the largest dune field in North America, would not be discernible at the resolu-

R. E. Arvidson, McDonnell Center for the Space Sciences, Department of Earth and Planetary Sciences, Washington University, St. Louis, MO 63130.
V. R. Baker, Department of Geosciences, University of Arizona, Tucson, AZ 85721.
C. Elachi and R. S. Saunders, Jet Propulsion Laboratory, 4800 Oak Grove Drive, Pasadena, CA 91109.
J. A. Wood, Smithsonian Astrophysical Observatory, 60 Garden Street, Cambridge, MA 02139.